Water Mass Formation from Revised COADS Data

KEVIN G. SPEER

Laboratoire de Physique des Océans, IFREMER, Plouzané, France

H.-J. ISEMER

Institute for Atmospheric Physics, GKSS-Research Center, Geestacht, Germany

A. BIASTOCH

Institut für Meereskunde, Kiel, Germany

11 May 1994 and 1 February 1995

ABSTRACT

Surface heat and freshwater fluxes from the Comprehensive Ocean–Atmosphere Data Set are revised and used diagnostically to compute air–sea transformation rates on density, temperature, and salinity classes over the domain of the data. Maximum rates occur over the warmest water and over mode waters, which are the dominant result of air–sea interaction. Transformation in different oceans is accordingly distinguished by temperature and salinity, just as water masses in different oceans are so distinguished. Over the entire domain, to about 30°S, approximately 80×10^6 m^3 s^{-1} of warm and cool water are transformed by air–sea fluxes, on annual average. Calculations for several seas in the North Atlantic, where deep water is thought to originate, are also presented.

1. Introduction

Air–sea heat and freshwater fluxes modify the temperature and salinity of water near the surface of the ocean. Despite the enormous range of space and time scales of this forcing, certain water masses form of more or less restricted temperature and salinity classes. These water masses by definition are distinguished by their exceptional volume compared to that in neighboring temperature and salinity classes (Worthington 1981). The foremost sorting mechanism at work is gravity, which tends to spread thin buoyant layers over denser layers in the ocean. Once created, the layers tend to preserve their stratification in the absence of further forcing to an extent determined by vertical stretching or compression and internal mixing. These tendencies are captured in a conservation equation for large-scale potential vorticity, a quantity that has been used to track water masses formed in deep-mixed layers (e.g., Talley and McCartney 1982; McCartney 1982; McDowell et al. 1982).

While the role of air–sea fluxes in producing the deep mixed layers and forming mode waters is evident, the relative contribution of this forcing compared to internal adjustment and mixing is unclear. For instance, eddy fluxes are thought to be capable of homogenizing potential vorticity over large regions, in effect redistributing a water mass laterally. If the bulk of this water mass is made virtually uniform on a regular basis by air–sea fluxes, then the large-scale role of the eddy fluxes could be greatly reduced. They may only act to remove local anomalies. In the opposite extreme, a small-scale, localized forcing by air–sea fluxes may have its influence carried over a large region by wind-driven currents and the propagation of planetary waves. A goal of this study is to attempt to quantify the degree of forcing by focusing on the distribution of air–sea fluxes over sea surface temperature, salinity, and density. That is, the distribution of air–sea fluxes over the surface expression of specific water masses.

A further motivation is to go beyond integrated measures of thermal and haline forcing used to test ocean models and deal directly with water masses. Water masses are the largest coherent thermohaline structures whose causes may be investigated. Many different physical mechanisms of heat, salt, and mass transport, as well as stratifications, are consistent with realistic meridional heat, salt, or freshwater flux. General circulation models are likely to get reasonable integrated fluxes with reasonable forcing but are unlikely to get mode waters correct, for instance, without an accurate representation of these mechanisms. To begin to con-

Corresponding author address: Dr. Kevin G. Speer, Laboratoire de Physique des Océans, IFREMER, B.P. 70, 29280 Plouzané, France.
E-mail: Kevin.Speer@ifremer.fr

TABLE 1. Comparison of revised and unrevised data. Minimum, maximum, and mean computed with all available datapoints.

	Source	Unit	Min	Max	Mean	Points
SST	COADS	°C	1.17	29.4	21.0	28 602
SST	Levitus	°C	−1.96	29.7	16.6	35 094
SSS	Levitus	psu	4.64	40.8	34.6	35 094
HEAT (unrev)	COADS	W m^{-2}	−203.7	116.7	1.84	26 062
HEAT (rev)	COADS	W m^{-2}	−229.3	202.4	−3.18	25 460
EVAP (unrev)	COADS	mm mo^{-1}	5.1	226.2	100.5	25 839
EVAP (rev)	COADS	mm mo^{-1}	0.0	273.3	134.6	25 464
RAIN	COADS	mm mo^{-1}	0.2	370.4	87.0	40 473
RAIN	Dorman	mm mo^{-1}	1.4	470.0	110.5	1620

strain these mechanisms, something in between bulk indices like meridional heat flux and the full details of local fluxes is needed. A diagnostic analysis of air–sea forcing is presented here, which may be thought of as a step toward a thermodynamic analysis of water mass formation.

The analysis derives from Walin (1982), who discussed formally the relation between surface heat flux and cross-isotherm advective and diffusive fluxes. The advective and diffusive fluxes may be integrated over the entire surface area of isotherms and balanced by an air–sea heat exchange of the form

$$\delta T \frac{\partial}{\partial T} \int_{A(T)} H dA, \qquad (1)$$

which is simply the net heating over the outcrop band $T \pm \delta T/2$. Here H is the heat flux and A is the region of the ocean surface of temperature less than T at a given time (see the appendix). Tziperman (1986) built a deep circulation model around a similar density flux forcing; Speer and Tziperman (1992) and Tziperman and Speer (1994) discussed the air–sea forcing of the North Atlantic Ocean and the Mediterranean Sea. Both applications show strong forcing at the densities of real water masses.

The question of whether advective or diffusive fluxes balance this forcing and where they occur, near the surface, deep in the interior, or near the bottom, is obviously a key one for the issue of physical mechanisms relevant to the thermodynamics. Walin (1982) pro-

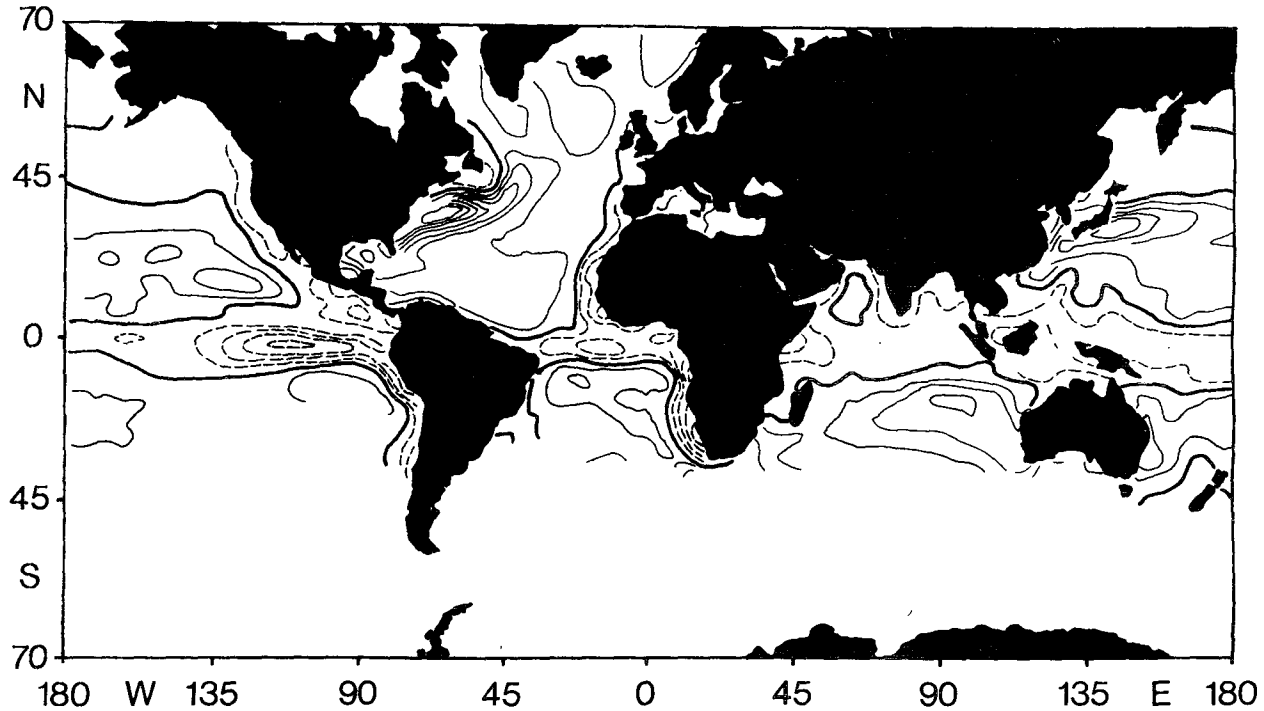

FIG. 1. Revised COADS annual mean density flux (10^{-6} kg s^{-1} m^{-2}). Contour interval 2.0, from a minimum of −8 to a maximum of 16 (negative values dashed).

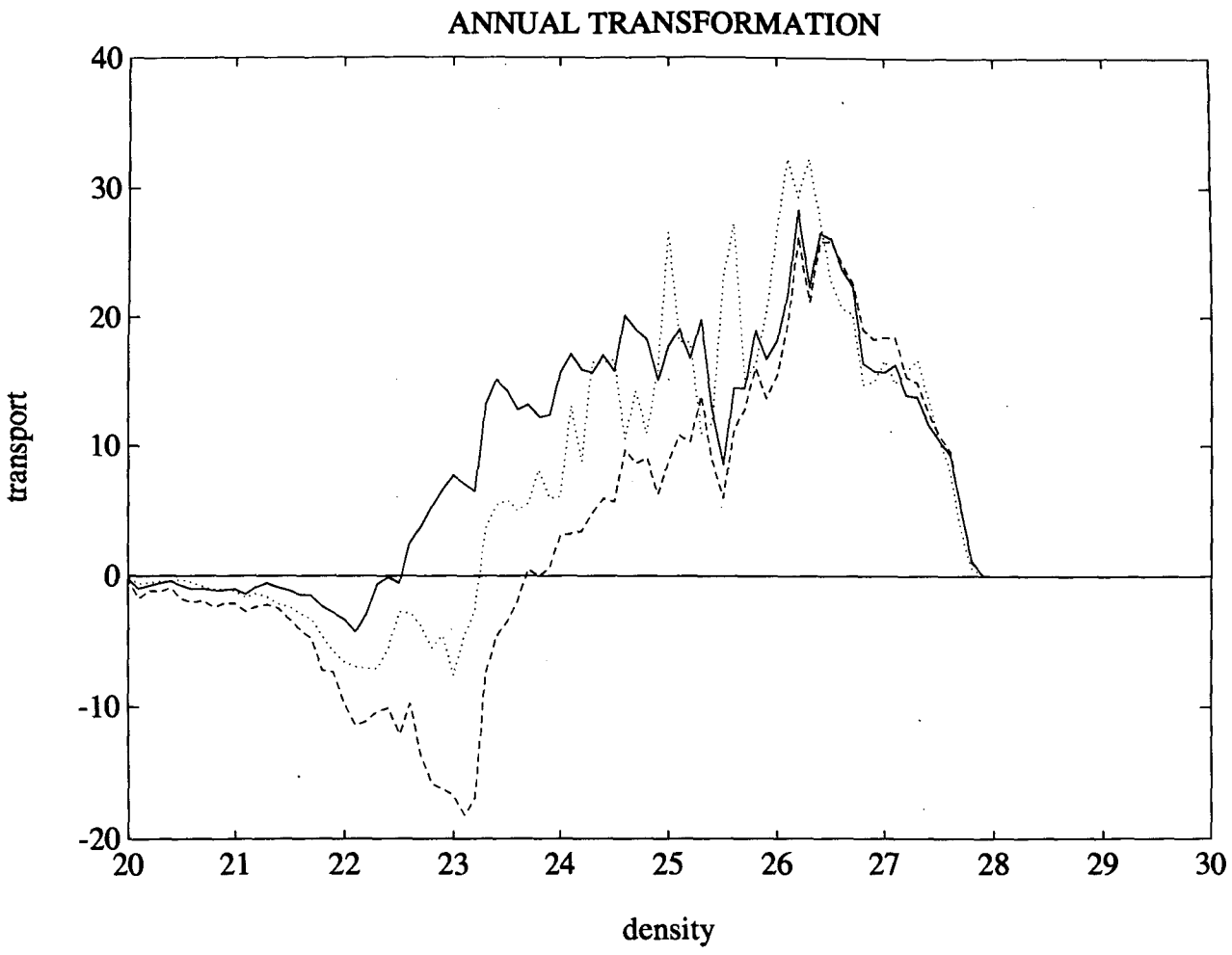

FIG. 2. Annual transformation (10^6 m^3 s^{-1}) versus sea surface density (kg m^{-3}) over the North Atlantic: comparison of Isemer and Hasse (1985) (dotted), unrevised COADS (dashed), and revised COADS (solid). Positive values correspond to buoyancy loss.

posed a formalism to distinguish between interior and boundary diffusive fluxes to illustrate the latter's importance in tropical surface layers. Speer (1993) noted that transformation measures advection for an idealized mixed layer. Garrett et al. (1995) have examined the question in the context of the Phillips (1966) Red Sea circulation model and have shown in detail how advective fluxes in a surface mixed layer can be balanced by air–sea forcing in the absence of horizontal mixing. Our purpose here is not to determine the circulation but to investigate quantitatively the role of air–sea fluxes in generating warm and cold water masses.

2. Data and method

The raw meteorological parameters of the Comprehensive Ocean-Atmosphere Data Set (COADS, Woodruff et al. 1987) were analyzed by Wright (1988) and Oberhuber (1988) to produce the monthly climatological air–sea fluxes of heat, rainfall, and evaporation used in this study. Sea surface temperature and salinity are needed for the calculation in density classes. Results were computed using both COADS and Levitus (1982) SST, and Levitus sea surface salinity (SSS). Comparisons were made with other data sources (Esbensen and Kushnir 1981; Isemer and Hasse 1987) to investigate the range of error in the calculation. The resolution in time and space varies from one dataset to another; to aid comparisons all data were interpolated to a monthly 1° × 1° grid.

Known errors in historical wind measurements (Cardone et al. 1990; Isemer and Hasse 1991) led us to revise statistically the calculated monthly means (not the raw meteorological parameters) essentially to mimic the correction applied by Isemer et al. (1989) to historical North Atlantic Ocean data. The most important change is the increased evaporation though revised wind speeds, resulting in a greater cooling and salinification of surface waters (Table 1). The density flux is defined by

$$H^{\rho} = -\frac{\alpha H}{c_p} + \frac{\beta S \rho(T, 0)(E - P)}{1 - S}, \qquad (2)$$

where H is the heat flux, α and β are the expansion and contraction coefficients, ρ is density, and $E - P$ is evaporation minus precipitation. The annual mean (Fig. 1) shows density loss or buoyancy gain essentially confined to upwelling areas on the equator, along eastern boundaries, and in the Indian Ocean. A broader, weaker loss also occurs in the northern Pacific Ocean. Density gain, mainly due to cooling, is concentrated near western boundaries and in the transoceanic drift into subpolar gyres.

A detailed comparison of revised COADS to other datasets covering only the North Atlantic Ocean illustrates the greatly reduced low-latitude buoyancy gain (Fig. 2) owing to increased evaporation. At higher latitudes (or high densities) the results are very similar for all recent datasets. Integrating over all densities to get the average value over the whole ocean gives a result, however, that is sensitive to the choice of dataset (Table 2).

The details of the calculation have been presented in earlier studies; a brief summary is provided in the appendix. The calculation essentially consists of integrating air–sea heat and freshwater fluxes over surface temperature and salinity classes, much like a water mass census but of fluxes rather than volume. The result can be expressed as a transport because a given input of heat or freshwater is capable of modifying the temperature and salinity of a volume of water at a certain rate according to its specific heat and initial salinity.

It may be helpful to consider the relation between transformation F (see the appendix), formation $-dF/d\rho$, and subduction under simplifying assumptions about diabatic effects. The subduction is a *local* quantity defined as the rate at which water crosses a control surface at the base of the mixed layer to enter the thermocline. Simplified mixed layer models have led to expressions for subduction involving the surface fluxes (e.g., Nurser and Marshall 1991). Key assumptions are the absence of horizontal mixing and an adiabatic thermocline. Such conditions also lead to an equality between F and horizontal flow near the surface (Walin 1982; Speer 1993; Garrett et al. 1995). Under these assumptions and for the steady state, integrating subduction $S(x, y)$ over an isopycnal outcrop gives the difference in F from one side to the other of the outcrop, or $-dF/d\rho = S(\rho)$ in the limit of small density difference. It should be emphasized that F has meaning as an air–sea interaction quantity independent of any assumptions regarding mixing; however, its interpretation *as circulation* naturally depends on such assumptions.

In the steady situation the water entering the interior does not change the volume of water at a given density, because mixing evacuates the volume at the same rate. At the opposite extreme, air–sea interaction events may create a new volume of dense water. Consider a limited area A over which a buoyancy flux B acts to produce water with a buoyancy anomaly $g' = B\tau/H$, where τ is the duration of the event and H is a fixed mixed-layer depth scale. In this situation the formation calculation scales like $BA/g' = HA/\tau$, or volume of new water produced per timescale. In our calculation with climatological data the shortest event lasts one month. More rapid events are to some extent averaged into the datasets; our working assumptions are that the datasets reflect the basic regional and seasonal variation of sea surface conditions and that they merit investigation despite errors (see the appendix).

3. Results

a. Global to 30°S

A buoyancy input at low densities, represented by negative values (Fig. 3a), occurs mainly over tropical

TABLE 2. Comparison of revised COADS data to other datasets for the North Atlantic, calculated from the annual mean data. The area used for total transport of heat or water at the surface is that up to 65°N (50.7×10^6 km^2).

	Min	Max	Mean	Mean × area (PW)
1. Net downward heat flux (W m^{-2})				
COADS unrevised	−203.7	85.0	−14.5	−0.90
COADS revised	−229.3	102.5	−19.1	−0.97
Isemer and Hasse	−249.5	142.3	−22.0	−1.12
Esbensen and Kushnir	−144.6	84.0	−0.3	−0.02
	Min	**Max**	**Mean**	**Mean × area (Sv)**
2. Evaporation (mm mo^{-1})				
Unrevised COADS	18.9	226.2	99.3	1.9
Revised COADS	28.2	273.4	131.2	2.5
Isemer and Hasse	21	315	140.5	2.7
3. Rainfall (mm mo^{-1})				
COADS	1.7	276.7	87.5	1.7
Dorman and Bourke	2	272.0	80.0	1.5

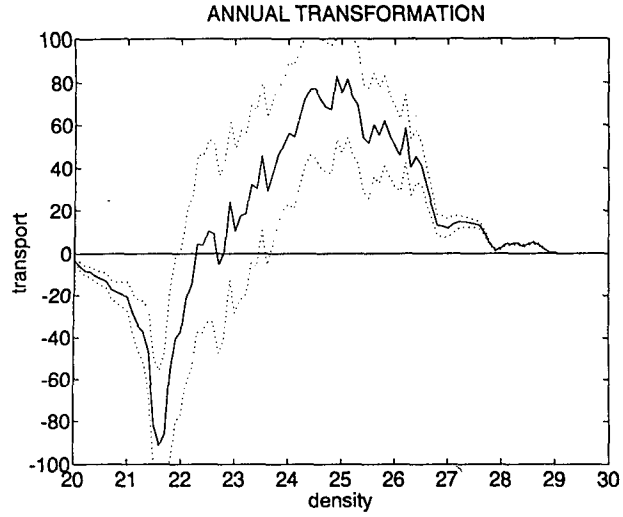

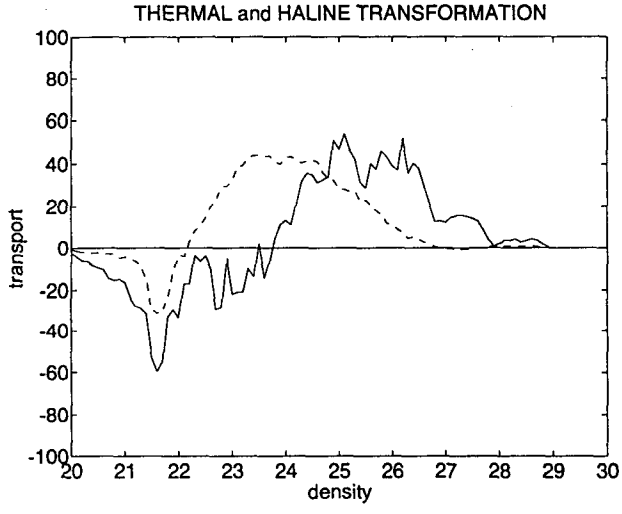

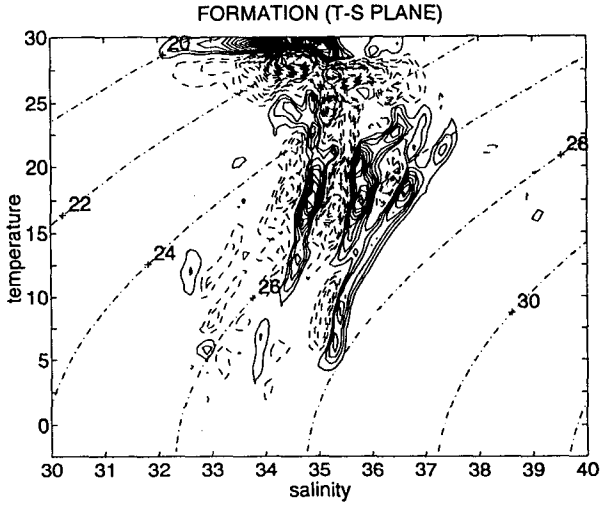

warm water with temperature greater than 25°C. The maximum buoyancy loss near $\sigma = 25$ (sea surface density anomaly, kg m^{-3}) occurs at sea surface temperatures of about 20°C. This density or temperature outcrops at latitudes roughly 30°N and 30°S (Levitus 1982), typically underneath the center of the subtropical atmospheric high pressure system that blows warm surface water poleward to be cooled. At higher densities the transformation drops off, most clearly at densities just below $\sigma = 27$, which lies within the main thermocline over most of the World Ocean. The range from 25 to 27 lies on the poleward side of the subtropical gyres of all the oceans (and covers both the subtropical gyre and the subpolar gyre in the North Pacific). Another drop occurs near 28, across the subpolar gyre of the North Atlantic Ocean (Fig. 3b; Speer and Tziperman 1992). At the highest sea surface densities there is the conversion of Atlantic inflow into dense salty water that eventually flows out of the Mediterranean Sea (Tziperman and Speer 1994; see also Fig. 5). The amplitude of transformation over the entire domain of the COADS dataset (see Fig. 1) varies from -90×10^6 m^3 s^{-1} near $\sigma = 21.5$ to 80×10^6 m^3 s^{-1} near $\sigma = 25$ (Fig. 3a).

The transformation maximum near $\sigma = 25$ of 80×10^6 m^3 s^{-1} toward higher densities is the sum of roughly 35×10^6 m^3 s^{-1} from the Pacific Ocean, 25×10^6 m^3 s^{-1} from the Atlantic Ocean, and 20×10^6 m^3 s^{-1} from the Indian Ocean. Walin (1982) obtained a similar total transformation from climatological data analyzed by Andersson et al. (1982). These numbers are also estimates for the total subtropical and subpolar thermocline water formation $[F(25) - F(\rho_{max})]$ by air–sea fluxes for each ocean since the transfer across $\sigma = 25$ converges at higher densities. This includes transformation over density ranges that are outside the usual definitions of mode waters. Unfortunately, large areas of the Southern Hemisphere subtropical domain, as well as the entire southern subpolar domain, are missing. The numbers for the North Atlantic (25×10^6 m^3 s^{-1}) and North Pacific (20×10^6 m^3 s^{-1}) alone account for much of the transfer (see Figs. 2, 3d), so the total magnitude would be somewhat greater if the subtropical gyres of the South Atlantic and South Pacific were fully represented.

The huge area of the tropical Pacific gives it the dominant contribution to worldwide warm water transformation, at nearly 80% of the total (Fig. 3b). The next greatest contribution comes from the Indian Ocean (Fig. 3c), and finally the Atlantic Ocean (Fig. 3b).

FIG. 3a. Annual transformation (10^6 m^3 s^{-1}) versus sea surface density (kg m^{-3}) from revised COADS data, worldwide (top). Dotted curves obtained by adding and subtracting 10 W m^{-2} at each point. Thermal ($\beta = 0$) and haline ($\alpha = 0$) components (middle). Annual formation over T–S classes (0.5°C × 0.1 psu); contour interval 0.5 × 10^6 m^3 s^{-1} (bottom).

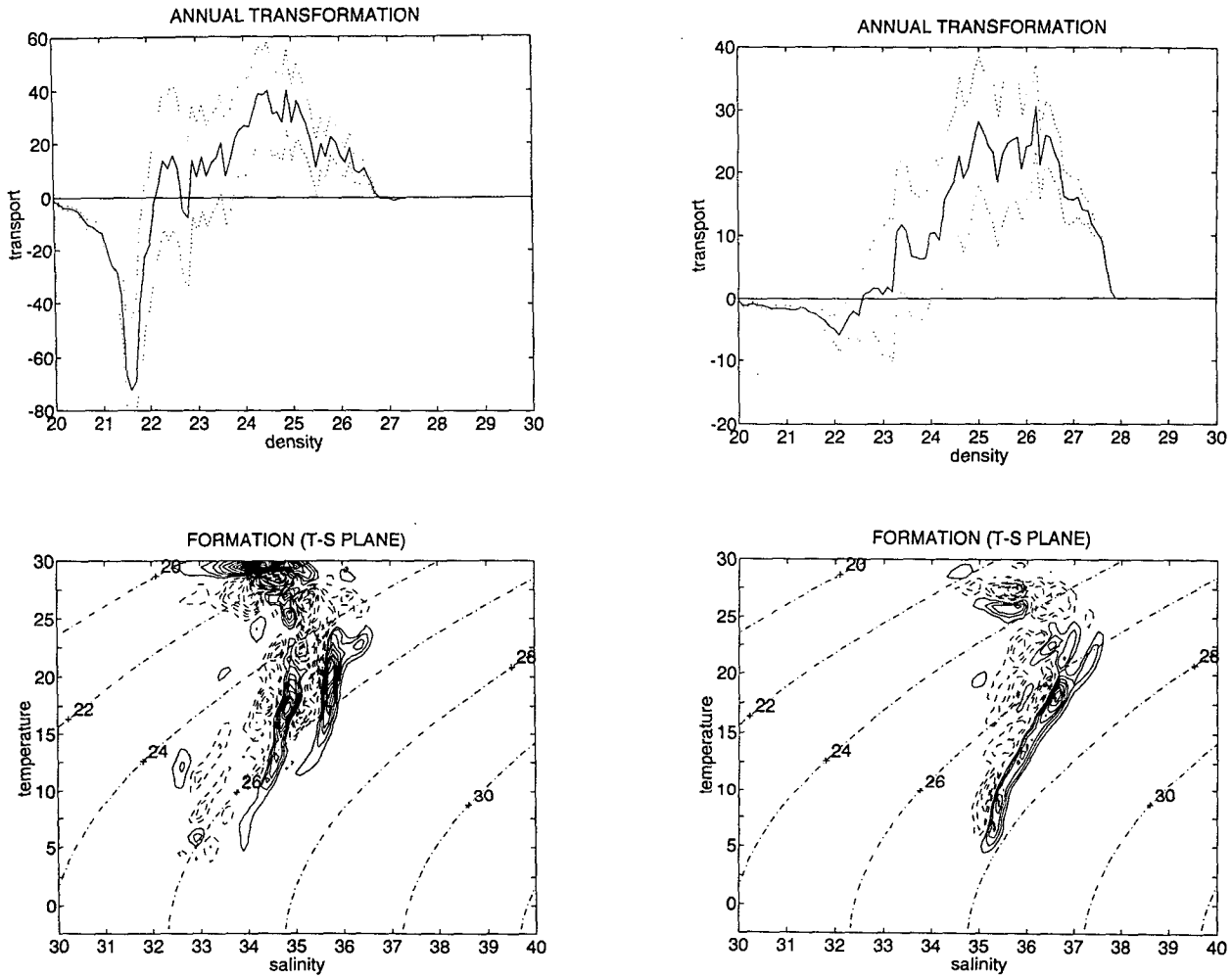

FIG. 3b. Annual transformation (10^6 m^3 s^{-1}) in Pacific (left) and Atlantic (right) (see Fig. 1 for coverage). Contour interval on T–S plane 0.5 × 10^6 m^3 s^{-1}.

Both thermal (2/3) and haline (1/3) components increase the buoyancy of the warm water (Fig. 1). These ratios are quite different in the Indian Ocean though, where the net precipitation is weaker (Fig. 3c) at low density. It is notable that, for the World Ocean as a whole, the thermal and haline forcing are of similar strength in the density range of water above the main thermocline. At higher density, the relatively weak haline component is nevertheless important; however, because of its systematic effect on salinity in limited regions (for instance, net precipitation in subpolar gyres and evaporation in the Mediterranean Sea) the amount of water involved in such conversion is small on the global scale.

A small contribution from the Mediterranean Sea does show up on the distribution of formation over temperature and salinity classes near 16°C, 39 psu, 29 kg m^{-3}, but it is dwarfed by other regions (Fig. 3a). The strongest of these is again the formation of the warmest water, mainly in the Pacific, at temperatures greater than 27°C. The low-latitude subsurface salinity maximum water at densities centered around 25 can be traced to the surface, where the salinity maxima occur in the density range 24–25.5 (Levitus 1982); this evaporation-driven modification is reflected in the formation of the highest salinity water near 20°C in all of the oceans (Fig. 3a).

A striking aspect of formation in temperature salinity classes is the separation by salinity into three prongs or ridges of formation. This is reminiscent of Worthington's (1981) warm water volumetric analysis for the World Ocean (Fig. 4). The correspondence is no accident, as the high volume classes are essentially mode waters consisting of thick mixed layers formed by wintertime convection. On the global scale, the dominant net annual air–sea interaction leads to the generation of these mode waters as well as the warm water pool.

Subantarctic mode water (McCartney 1977) is an important component of the volumetric census at temperature from 14° to 4°C (Worthington 1981) but, as

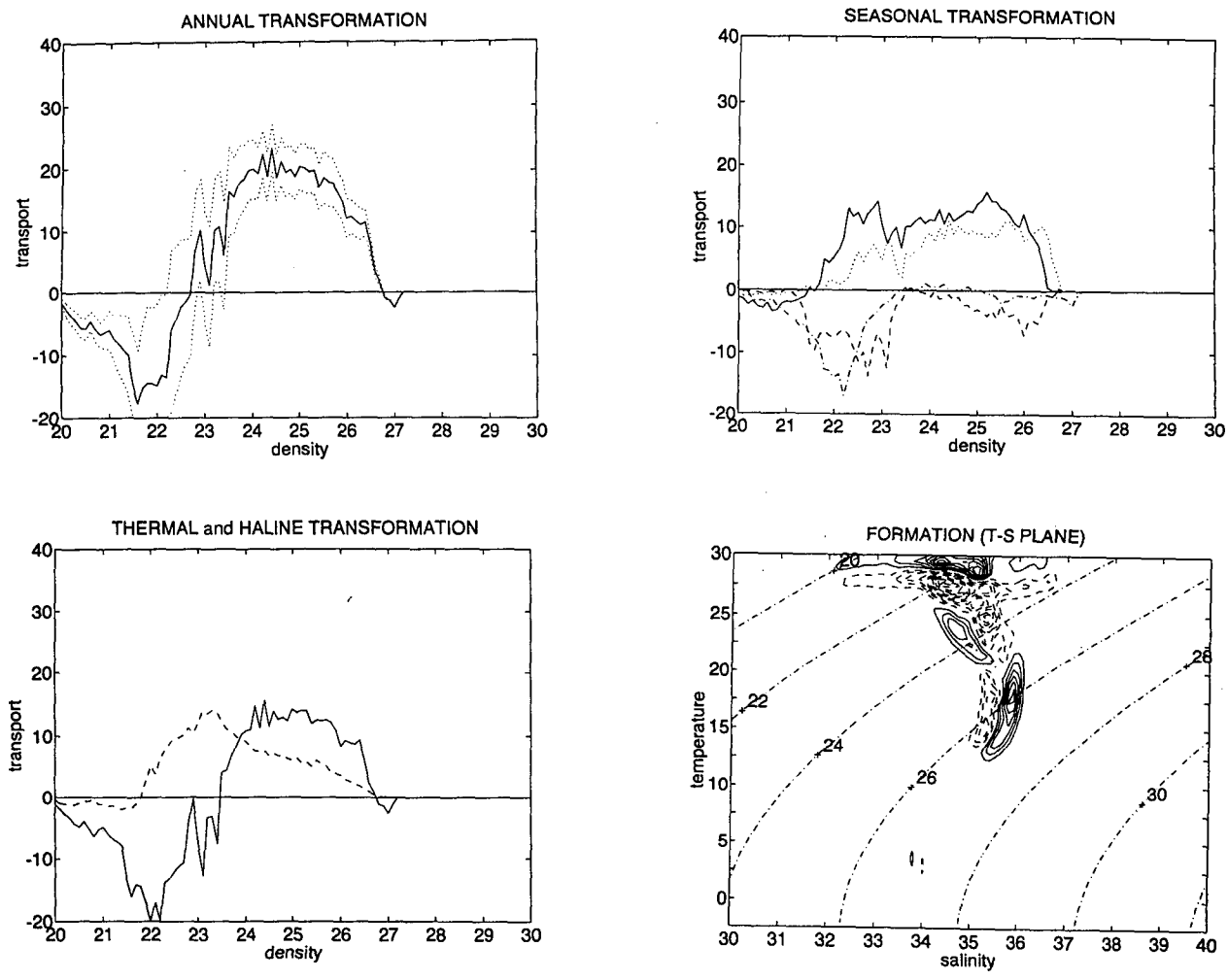

FIG. 3c. Annual transformation (10^6 m^3 s^{-1}) for the Indian Ocean (see Fig. 3a). Seasonal components: A–M–J (solid), J–A–S (dotted), O–N–D (dashed), and J–F–M (dash–dot).

mentioned above, the Antarctic region is missing from the COADS dataset. Preliminary calculations reflect simply the climatology of the region, with a heat loss to the north of the Polar Front and heat gain to the south (Esbensen and Kushnir 1981). The net buoyancy input occurs south of the Polar Front apparently owing to eddy air–sea fluxes (Taylor et al. 1978); this effect magnifies formation in the vicinity of the front by heating water on the cold side and cooling it on the warm side. However, given the present large uncertainties in the fluxes in this region, we do not attempt to quantify this formation.

b. Marginal North Atlantic seas

Calculations are presented for regions of special interest to deep water formation in the North Atlantic Ocean: the Labrador Sea and the Nordic seas (the Norwegian Sea, Greenland Sea, and Iceland Sea; Fig. 5). An analysis of formation by air–sea fluxes in the Mediterranean Sea has already been presented by Lascaratos (1993), including the spatial distribution, and by Tziperman and Speer (1994). The latter included box models to investigate the role of the seasonal cycle. Certainly many other regions in other oceans deserve detailed study as well. Limiting the calculation to an open region invalidates the connection to the full oceanwide mass and heat budgets of isothermal or isopycnal layers but still represents the contribution of a particular region and may illuminate the special air–sea interaction taking place there.

In the Labrador Sea (defined here as the northwest Atlantic to 50°N and east to 40°W) the spring, summer, and fall transformations more or less cancel leaving the wintertime magnitude of about 1×10^6 m^3 s^{-1} (Fig. 5a). There is a weak compensating precipitation effect (note that ice and runoff are not included) but the main forcing is thermal. Labrador Sea Water is thought to be formed with the characteristic temperature and salinity of 3.4°C and 34.9 psu (Lazier 1973). Pickart (1992)

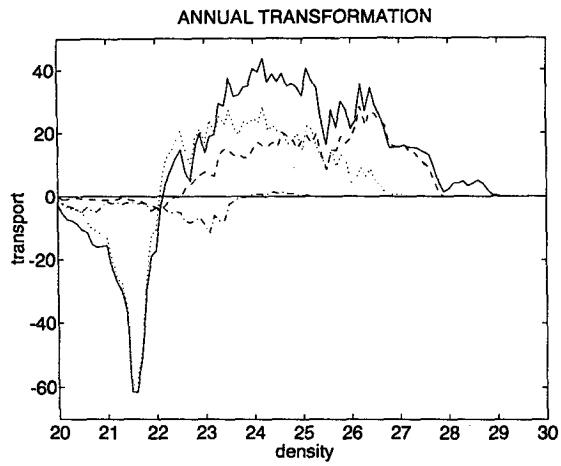

FIG. 3d. Annual transformation (10^6 m^3 s^{-1}) for Northern Hemisphere oceans from revised COADS data (solid); NATL (dashed), NPAC (dotted), and NIND (dash–dot).

has described a variety thought to be more strongly ventilated, based on higher Freon concentrations, with temperature 4°–5°C and salinity of roughly 34.8 psu when formed (Upper Labrador Sea Water). The formation calculated here from climatological data is maximum at 2.5°C, 34.7 psu, 27.7 and 5°C, 34.7 psu, 27.4. The cold peak trails off in positive formation at very cold, fresh Labrador Current values, while the formation of the densest water occurs at slightly warmer and saltier values across $\sigma = 28$. Both of these maxima appear to be too fresh to match the characteristics of water masses found in the upper 2000 m of the Labrador Sea; however, smoothed data seem likely to bias results to fresh values near boundaries where there are extremely fresh currents. Also, both Lazier (1973) and Pickart (1992) noted the importance of mixing between Labrador Sea sources and the saline North Atlantic Current to raise initial salinities to observed values. Evidently this lateral mixing is a basic part of the formation process in the Labrador Sea, unlike 18° Water in the subtropical gyre, for example, together with direct formation by surface fluxes.

The formation maximum near 5°C and 34.7 psu is interesting, but where does the formation take place? The central part of the sea is excluded because density is too high there. By simply mapping the location of the most intense air–sea fluxes (essentially heat flux) on surface water with the T–S values in the neighborhood of the 5°C formation maximum, the likely region of formation may be found. This turned out to be the Irminger Sea, south and east of Greenland, at the northern entrance to the Labrador Sea (Fig. 6). Thus, the 5°C maximum represents the formation of subpolar mode water at these T–S values. Pickart (1992) argued that this water mass is not the source of Upper Labrador Sea Water because it is too salty and would be relatively low in Freon by the time it made it around the Labrador Sea and down the western boundary, suggesting instead that convection occurs off the Labrador coast, which mixes quite fresh surface water with deeper water. If we broaden our search to include SSS values as fresh as 33 psu (Fig. 5a), then we do find strong air–sea interaction taking place in the southern Labrador Sea, inshore of the North Atlantic Current (Fig. 6). This is one of the regions identified by Pickart (1992) as a likely region of formation.

Our results taken strictly imply that convection in the Irminger Sea supplies the bulk of the water near 5°C, though our failure to find strong fluxes in the southern region *at the SSS of positive formation* may be the result of poor climatology in a region of strong gradients. Intriguingly, strong fluxes nevertheless are found in the south at the right temperatures, at least suggesting that this water mass is subsequently modified by injections of relatively fresh, high-Freon water in the southern Labrador Sea. Detailed study is needed to determine the relative contribution of the two sites.

A secondary maximum occurs near 8°C, 34.6 psu, 27.0 (Fig. 5a). Such characteristics occur east of the Grand Banks near 43°N in data reported by Clarke et al. (1980), who refer to several author's descriptions of this low-salinity intermediate water, which sinks into the northern edge of the North Atlantic Current (see also Harvey and Arhan 1988). Worthington (1976), for instance, displayed a low salinity anomaly near 50°N at temperatures from 5°–10°C. Fuglister (1960) shows very low salinity water entering the thermocline at somewhat cooler temperatures, 5°–8°C, in the western part of his 48°N section. The results of the calculation in the Labrador Sea box, through which part of the North Atlantic Current passes, suggest that a variety of intermediate waters are formed by air–sea fluxes.

The Nordic Sea's annual transformation has a simple structure representing the conversion of warm Atlantic

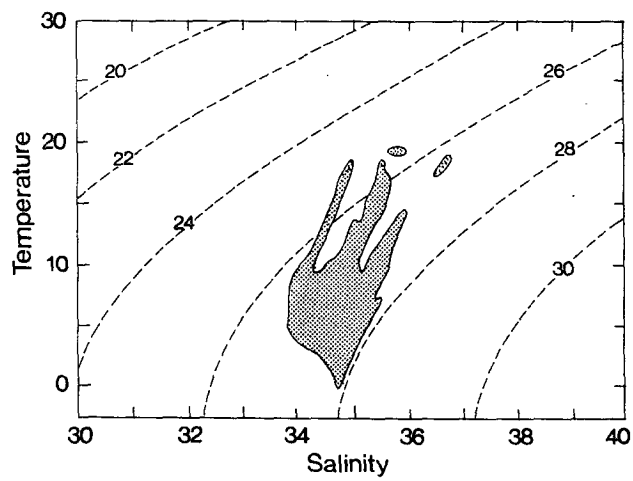

FIG. 4. Temperature and salinity classes (0.1°C × 0.01 psu) of the World Ocean with volume greater than 5 × 10^3 km^3 (shaded) from Worthington (1981). Principal components of the three high-volume ridges warmer than 10°C are from the North Pacific (fresh), subtropical Southern Hemisphere (central), and North Atlantic (saline).

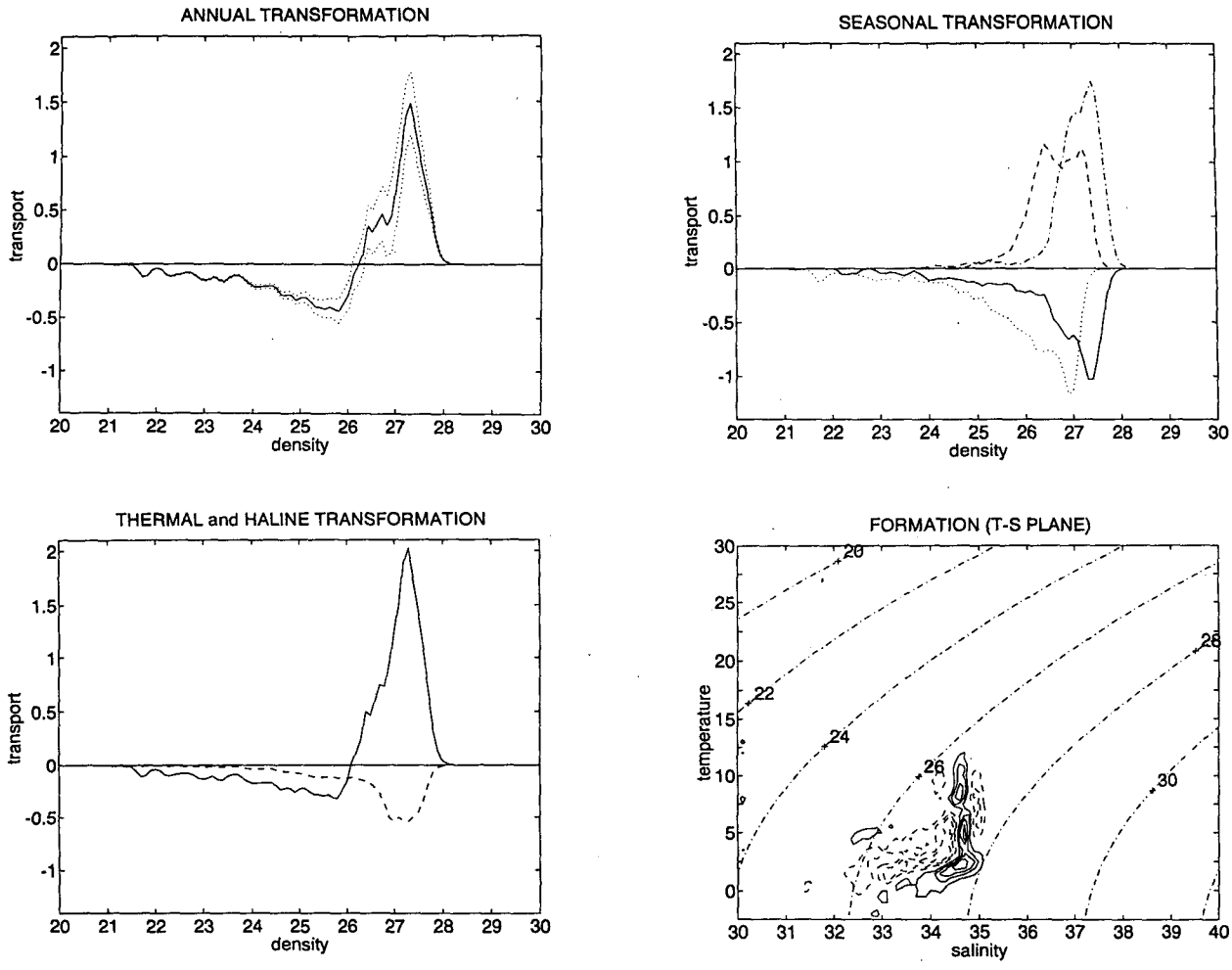

FIG. 5a. Transformation (10^6 m^3 s^{-1}) in Atlantic seas (see caption to Fig. 3). Labrador Sea (contour interval 0.05 × 10^6 m^3 s^{-1}).

Water into a cooler version of the same (Fig. 5b). Unfortunately, the freshening implied by inflow and outflow salinity differences is not represented in our dataset, which does not include runoff nor the arctic freshwater budget. Both fall and winter contribute about equally, while summer and spring contributions are relatively weak, so that the seasonal cycle is less pronounced than in other basins. Mauritzen (1994) noted the absence of a seasonal signal in the overflow and concluded that seasonality in the regional circulation was weak because Atlantic Water had a residence time of 2–3 yr in the Norwegian Sea in her circulation model, thus averaging out any signal. Here, the formation rate itself shows reduced seasonal variation.

The characteristics of dense water flowing out of the Nordic Seas vary from roughly 0° to 3°C and 34.9 to 35.0 psu (Worthington 1970, 1976), a rather wide range probably partially influenced by mixing near the outflow sill itself. If most of the transport in this flow is in the middle of the range, say 1°–2°C, the implied formation of such water is not apparent at even the smallest contoured value (0.25 × 10^6 m^3 s^{-1}, Fig. 5b). Lack of winter data would bias our results and degrade the resolution of this conversion; the climatological data shows primarily the strong interaction associated with the Norwegian Current (Swift and Aagaard 1981).

To investigate data resolution issues in the Nordic Seas, COADS was compared to the original Bunker dataset interpolated onto a 1° × 1° grid in order to use the full hydrographic spatial resolution. Bunker's averaging boxes were larger than the COADS; hence, there are none missing from lack of data. In this way more of the sea was resolved, though at the price of less spatial structure to the fluxes. The results using Bunker's data do show formation at the lower temperatures (Fig. 7). These results agree qualitatively with Swift et al.'s (1980) surface layer volume changes from October 1974 to March 1975.

The total volume change from Swift et al. (1980) for intermediate water is 13 090 km^3. Over the four-month period between observations this amounts to a rate of 1.3 × 10^6 m^3 s^{-1} on average. Summing the February formation (not shown) over the intermediate wa-

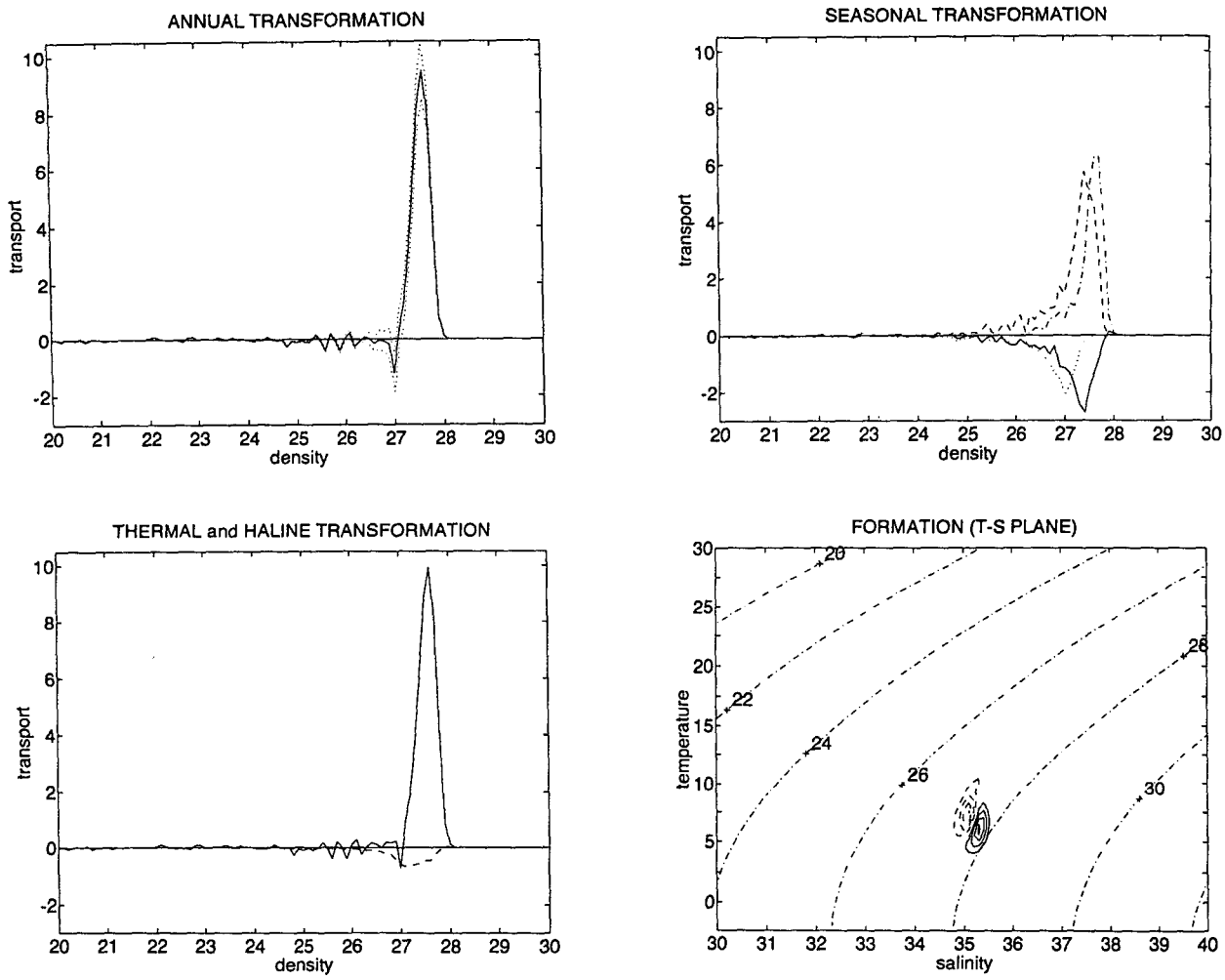

FIG. 5b. As in Fig. 5a but for Nordic Seas (contour interval 0.5 × 10^6 m^3 s^{-1}).

ter T–S range −1°–0°C and 34.8–35 psu we get 0.8 × 10^6 m^3 s^{-1} and 2.4 × 10^6 m^3 s^{-1} if the March contribution is added; these are the only winter months that contribute. So the observed rate of volume change lies within the range of air–sea flux estimates (ignoring mixing) for the climatological winter season. But does this cold water supply all of the dense overflow?

Estimates of dense outflow include 6 × 10^6 m^3 s^{-1} (Worthington 1970, 1976) at 1°C, 1.7 × 10^6 m^3 s^{-1} at 0°C (McCartney and Talley 1984), and 5.6 × 10^6 m^3 s^{-1} at density greater than 27.8 (Dickson and Brown 1993), so the cold water formation rates above appear to be inadequate. Mauritzen (1994) proposed a new circulation scheme in which the dense component of overflow is dominated by Atlantic Water cooled in the Norwegian Sea, which subsequently circulates isopycnally under the Arctic ice where it is modified into overflow water; overall, roughly 4 × 10^6 m^3 s^{-1} originates directly from Atlantic Water and only 1 × 10^6 m^3 s^{-1} from gyres north of Iceland (the cold intermediate water source).

Mauritzen's 5 × 10^6 m^3 s^{-1} total dense overflow component is probably comparable to our average value of transformation between 27 and 28 of about 4 × 10^6 m^3 s^{-1} (Fig. 5c) because the heat flux climatologies are similar and also because the average transformation represents an average cross-isopycnal transfer from 27 to 28—similar to her choice of inflow and outflow densities. This is a statement of the net buoyancy balance for the sea.

On the other hand, in special circumstances of negligible diapycnal mixing and steady flow (Garrett et al. 1995), the maximum transformation (9 × 10^6 m^3 s^{-1}) would be equal to the total inflow or exchange, because all the inflow occurs at a single density (neglecting water somehow entering and leaving at the same density, unaffected by air–sea fluxes). For comparison, Worthington (1976) estimated 8 × 10^6 m^3 s^{-1} flowing in. However, in a more realistic setting the relation between transformation and circulation is more complicated. For instance, Tziperman and Speer (1994) noted the influence in model calculations of a strong seasonal

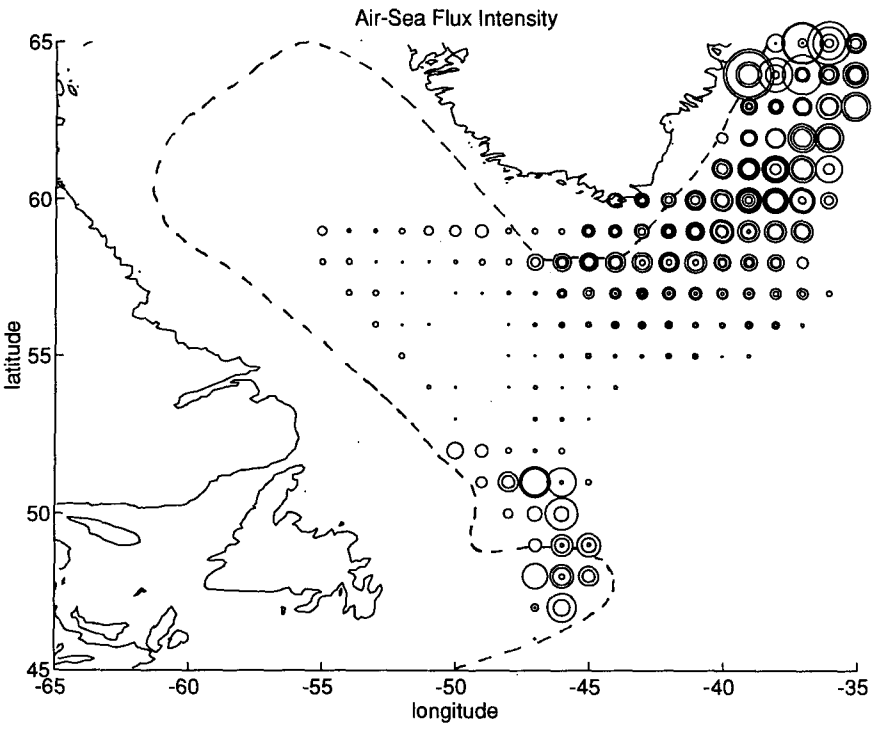

FIG. 6. Air–sea flux intensity in the Labrador Sea at selected months and T–S values. Radius of circles is proportional to the magnitude of the buoyancy flux, occurring at 4° < SST < 6°C, 33 psu < SSS < 34.95 psu, during the months of November–March. Interaction appears southeast of Greenland for SSS > 34.6 psu, but only appears in the southern Labrador Sea at fresher surface values (2000-m isobath dashed).

cycle together with mixing on the form and amplitude of transformation in the Mediterranean. The 9×10^6 $m^3\ s^{-1}$ maximum here represents a transfer by air–sea fluxes across $\sigma = 27.6$, but not, in general, the transport at the sill. Finally, data sampling and filtering problems are likely to be worse in regions of extreme weather, and this can lead to artificial or missing transformation. In any case, the estimates here do show the basic air–sea interaction taking place in the Nordic Seas and may help to determine which aspects of this interaction are most important to the circulation.

4. Discussion

The basic shape of the global climatological transformation curves arises from the nonuniform distribution of solar radiation over the earth, leading through atmospheric and oceanic circulation to net energy gain primarily in the Tropics, and loss elsewhere. The structure across the Antarctic Polar Front is an exception thought to be caused by local air–sea eddy heat exchange. A seasonal cycle also leads to a similar basic shape because air–sea heat exchange does not exactly cancel out at each density over the year, owing to advection and mixing during the creation and destruction of the seasonal thermocline.

The buoyancy gain in the Pacific Ocean is striking. Such gain implies an equally large role for turbulent mixing processes to eliminate the warm water. Storms are known to mix up the water beneath them (Leipper 1967). Nilsson (1994) has estimated transformation rates of the order of several million cubic meters per second on annual average for storms, insufficient to account for a significant part of the total even if there are 100 or so storms per year. Mixing under average conditions may be adequate, though (Niiler and Stevenson 1982).

The Pacific and Atlantic transformations are qualitatively similar despite the absence of deep water formation in the Pacific. Walin (1982) commented that this situation is a result of the similar meridional temperature gradient in each ocean, hence similar poleward drift of warm water. Here, the formation of mode waters or intermediate waters, qualitatively similar in both oceans, is emphasized. Most of the net oceanic energy loss occurs over recognizable water masses and makes deep mixed layers whose characteristics are often observed to spread across ocean basins.

Although our calculation allows us to describe quantitatively the air–sea flux driven component of water mass formation it does not explain this interaction; it does show that climatological fluxes systematically replenish contemporary water masses. This result does not imply that air–sea interaction is the sole reason for the persistence of mode waters, since ocean dynamics

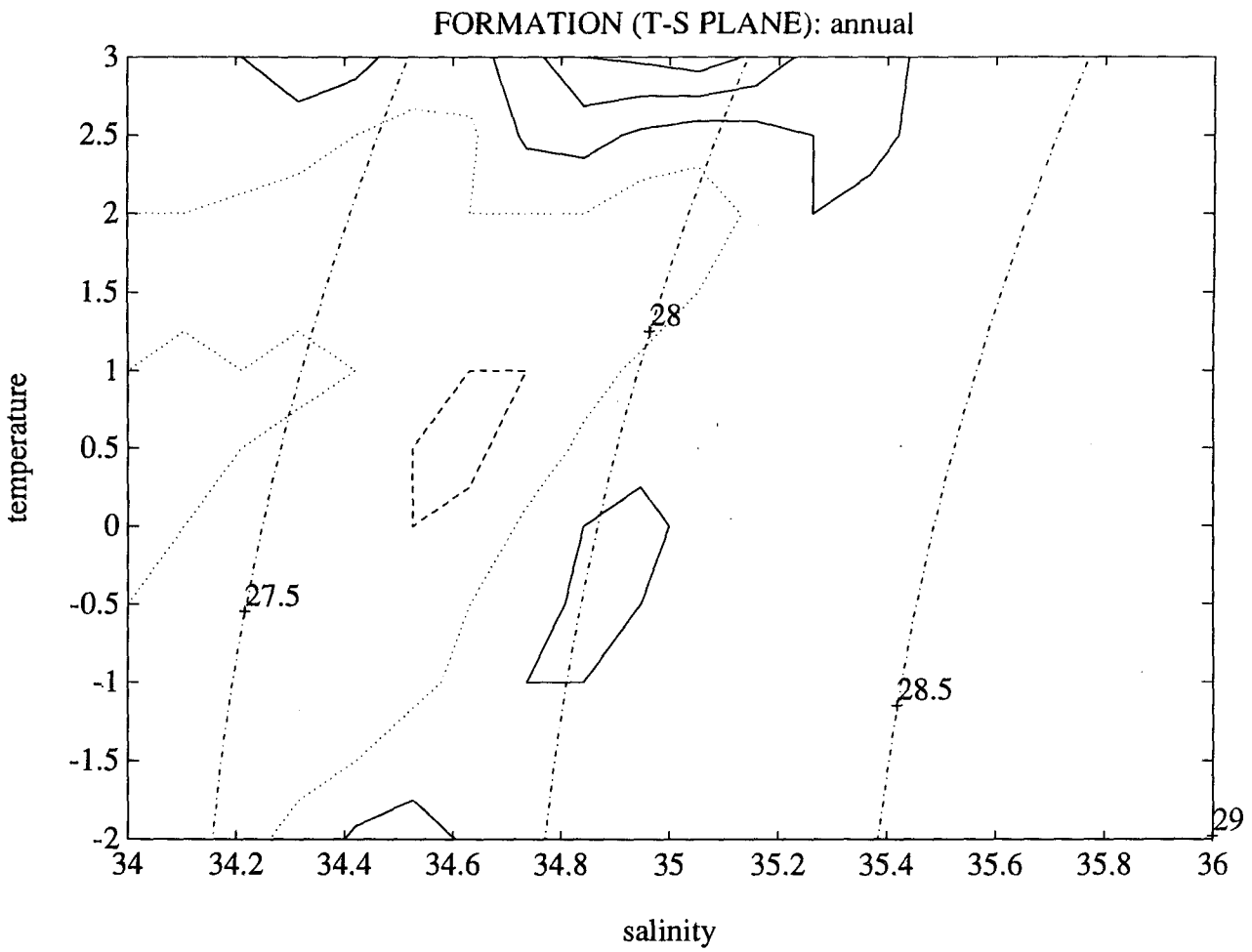

FIG. 7. Annual formation over cold T–S classes (0.5°C × 0.1 psu) in the Nordic Seas from Bunker data (contour interval 0.05×10^6 m^3 s^{-1}; positive values solid, negative values dashed, zero dotted).

can lead to a redistribution of thickness, but the calculation here does provide a quantitative basis for comparing various mechanisms.

One component of the ocean's stratification is generated by an overflow of dense water from marginal seas. This is almost invisible to our global-scale calculation that is dominated by the other component, mode water, plus warm water formation. No amount of surface data alone would allow us to estimate directly the formation of the two primary deep water masses, North Atlantic Deep Water, and Antarctic Bottom Water, because they do not exist anywhere at the surface. These are formed by relatively weaker net fluxes acting over shelfs and in marginal seas. The dense water thus created spills into the open ocean, mixing further (e.g., entraining) to become a major water mass. Their original volumetric contribution at the source can be relatively small because of their extreme characteristics, with mixing allowing volumes to expand internally, isolated from the surface.

General circulation models that form these water masses as deep polar mixed layers are, of necessity, effectively parameterizing entrainment. More importantly they are misdirecting the air–sea flux onto water types that do not really exist at the surface. Regional models have been designed specifically to resolve circulation in marginal seas, and one expects that the relatively well-known outflow characteristics will help to calibrate internal mixing parameterizations. Reproducing realistic transformation rates of particular water types should provide another sensitive test of model thermodynamics and parameterizations.

Acknowledgments. KGS received support from the Centre National de la Recherche Scientifique; AB received partial support for this work from a grant to G. Siedler. Shared observations by R. Pickart stimulated the Labrador Sea investigations.

APPENDIX

Method

The idea behind the calculation presented here is that by calculating the total density flux from the surface water to the atmosphere as a function of the density of the water loosing or gaining buoyancy rather than as a function of location it is possible to deduce the amount of water modified in any given density range by these fluxes. A detailed description of the calculation relating the surface density fluxes to water mass transformation is given in Andersson et al. (1982) (see also Walin 1982; Tziperman 1986; Speer 1993), and we shall only briefly describe it here.

Let the surface fluxes of heat and fresh water (evaporation minus precipitation) be $\mathcal{H}(x, y, t)$ and $\mathcal{W}(x, y, t)$, respectively. Both are functions of location and time, assumed to vary periodically with the seasonal cycle. Given the temperature and salinity of the surface water $T(x, y, t)$ and $S(x, y, t)$, it is possible to calculate the density flux as function of the surface density. The total density flux during one year, as function of the surface density, $F(\rho)$, is found from the above fluxes using the following expression:

$$F(\rho) = \int_{\text{year}} dt \iint_{\text{area}} dxdy \left[\frac{\alpha}{C_p} \mathcal{H}(x, y, t) - \frac{\rho(T, 0)\beta S}{1 - S}(x, y, t)\, \mathcal{W}(x, y, t) \right] \times \delta[\rho(x, y, t) - \rho'].$$

The delta function appearing in the integral is zero whenever the surface density is not equal to the density ρ, and therefore samples the surface buoyancy flux only for surface water of density ρ. Dividing by one year yields the annual average. For convenience, we call $F(\rho)$ the "transformation" and its derivative with respect to density the "formation." Both may be calculated as functions of the sea surface temperature and salinity as well.

Combining heat, salt, and mass conservation statements for fluxes across each isopycnal leads to a three-term balance:

$$F(\rho) + A(\rho) + \frac{dF_{\text{mix}}(\rho)}{d\rho} = 0,$$

where $A(\rho)$ is the advection across the isopycnal integrated over its surface area and $F_{\text{mix}}(\rho)$ is the integrated turbulent flux of density. In the case of a domain that includes all water of a given density in a steady state, the integrated advection over the total isopycnal surface cancels out, leaving mixing to balance forcing by air–sea fluxes.

Errors

Several studies have remarked on the impact of errors in the sea surface data on transformation. Tziperman and Speer (1994) argued that resolving sea surface density variations is more important than flux variations because fluxes tend to cancel at a given density, but that density is also likely to be sampled better. Walin's (1982) original estimate of worldwide transformation to greater density had an error of 40% attached, presumably based on observed differences between datasets used in the computation. Further comparison between Atlantic datasets (Speer and Tziperman 1992; this study) suggests a variation of 2×10^6 m^3 s^{-1} at high density (27–28), increasing to 10×10^6 m^3 s^{-1} at low density (22–23), or about 20%–100%. The strong variation at low density results from integrating moderate to weak fluxes susceptible to different flux parameterizations over large areas; the converse holding at high density. Assuming that recent climatologies are improvements implies that this variation overestimates the error. A plausible error seems to be 20%–50%.

Systematic uncertainties, due, for instance, to choices of parameterizations in bulk formulas, lead to different shapes of the transformation curve. This affects sensitively its derivative, the formation. Of particular importance to the shape is the trend in uncertainty with density. That is, fluxes over cool water have a different uncertainty than those over warm water. To demonstrate the trend, root-mean-square errors of several sources of uncertainty (Isemer et al. 1989) are tabulated (Table 3) as a function of latitude (a rough proxy variable for density). This trend has a magnitude of about 10 W m^{-2}, which is the basis for the bounding curves presented here in plots of transformation. We simply extrapolate this estimate to all oceans.

Errors in formation as a function of temperature and salinity are more sensitive to data coverage and are difficult to estimate as a function of T and S. We can only refer to flux errors in the region corresponding to a given surface water type. Note that integrating along isopycnals recovers the formation as a function of density, with the tendency for reduced error at high densities. We do not attempt to estimate the effects of missing data but observe that for the North Atlantic marginal seas the primary contributions come from regions (ice free) where relatively warm currents intrude and are subject to strong, persistent fluxes. (Quantitatively weaker interaction may still be important to property distributions.) Based on annual mean heat fluxes of roughly 70 ± 20 W m^{-2}, we expect errors of integrated quantities to be roughly 30%.

TABLE 3. Systematic uncertainty of net heat flux in latitude bands.

Latitude range	Uncertainty (W m^{-2})
6–10°N	31
16–20°N	30
31–35°N	28
41–45°N	26
51–55°N	19

In the South Pacific and South Atlantic extensive parts of the subtropical gyres are missing, so buoyancy fluxes and mode water formation there are underrepresented. Southern Ocean fluxes are the subject of current research.

REFERENCES

Andersson, L., B. Rudels, and G. Walin, 1982: Computation of heat flux through the ocean surface as a function of temperature. *Tellus,* **34,** 196–198.

Cardone, V. J., J. G. Greenwood, and M. A. Cane, 1990: On trends in historical marine data. *J. Climate,* **3,** 113–127.

Clarke, R. A., H. W. Hill, R. F. Reiniger, and B. A. Warren, 1980: Current system south and east of the Grand Banks of Newfoundland. *J. Phys. Oceanogr.,* **10,** 25–65.

Dickson, R. R., and J. Brown, 1994: The production of North Atlantic Deep Water: Sources, rates, and pathways. *J. Geophys. Res.,* **99,** 12 319–12 342.

Esbensen, S. K., and Y. Kushnir, 1981: The heat budget of the global ocean: An atlas based on estimates from surface marine observations. Climate Research Institute. Report n° 29. Oregon State University, Corvallis, OR, 27 pp., 188 charts.

Fuglister, F. C., 1960: Atlantic Ocean atlas of temperature and salinity profiles and data from the International Geophysical Year of 1957–1958. *Woods Hole Oceanographic Institution Atlas Series,* Vol. 1, 209 pp.

Garrett, C., K. G. Speer, and E. Tragou, 1995: The relationship between water mass transformation and the surface buoyancy flux, with application to Phillips's Red Sea model. *J. Phys. Oceanogr.,* **7,** 1696–1705.

Harvey, J., and M. Arhan, 1988: The water masses of the central North Atlantic in 1983–84. *J. Phys. Oceanogr.,* **18,** 1855–1875.

Isemer, H. J., and L. Hasse, 1987: *The Bunker Climate Atlas of the North Atlantic Ocean, Vol. 2: Air-Sea Interactions.* Springer-Verlag, 218 pp.

——, and ——, 1991: The Scientific Beaufort Equivalent Scale: Effects on wind statistics and climatological air-sea flux estimates in the North Atlantic Ocean. *J. Climate,* **4,** 819–836.

——, J. Willebrand, and L. Hasse, 1989: Fine adjustment of large scale air–sea energy flux parameterizations by direct estimates of ocean heat transport. *J. Climate,* **10,** 1173–1184.

Lascaratos, A., 1993: Estimation of deep and intermediate water mass formation rates in the Mediterranean Sea. *Deep-Sea Res.,* **40,** 1327–1332.

Lazier, J. R. N., 1973: The renewal of Labrador Sea Water. *Deep-Sea Res.,* **20,** 341–353.

Leipper, D. F., 1967: Observed ocean conditions and Hurricane Hilda 1964. *J. Atmos. Sci.,* **24,** 182–196.

Levitus, S., 1982: *Climatological Atlas of the World Ocean.* NOAA Prof. Paper 13, National Oceanic and Atmospheric Administration, Rockville, MD, 173 + XV pp.

Mauritzen, C., 1994: A study of the large-scale circulation and water mass formation in the Nordic Seas and Arctic Ocean. Ph.D. thesis, Massachusetts Institute of Technology and Woods Hole Oceanographic Institution, 212 pp.

McCartney, M. S., 1977: Subantarctic mode water. *A Voyage of Discovery, George Deacon 70th Anniversary Volume,* M. V. Angel, Ed., *Deep-Sea Res.* Suppl., 103–119.

——, 1982: The subtropical recirculation of mode waters. *J. Mar. Res.,* **40,** (Suppl.), 427–464.

——, and L. D. Talley, 1984: Warm-to-cold water conversion in the northern North Atlantic Ocean. *J. Phys. Oceanogr.,* **14,** 922–935.

McDowell, S., P. Rhines, and T. Keffer, 1982: North Atlantic potential vorticity and its relation to the general circulation. *J. Phys. Oceanogr.,* **12,** 1417–1436.

Niiler, P., and J. Stevenson, 1982: The heat budget of the tropical ocean warm-water pool. *J. Mar. Res.,* **40** (Suppl.), 465–480.

Nilsson, J., 1995: The impact of tropical cyclones on the ocean. Part II. Ph.D. thesis, University of Gothenburg, Sweden, 19 pp.

Nurser, A. J., and J. C. Marshall, 1991: On the relationship between subduction rates and diabatic forcing in the mixed layer. *J. Phys. Oceanogr.,* **21,** 1793–1802.

Oberhuber, J. M., 1988: An atlas based on the COADS data set: The budgets of buoyancy and turbulent kinetic energy at the surface of the global ocean. Max Plank Institute for Meteorology Report, N° 15, Hamburg, 200 pp.

Pickart, R. S., 1992: Water mass components of the North Atlantic deep western boundary current. *Deep-Sea Res.,* **39,** 1553–1572.

Phillips, O. M., 1966: On turbulent convection currents and the circulation of the Red Sea. *Deep-Sea Res.,* **13,** 1149–1160.

Speer, K. G., 1993: Conversion among North Atlantic surface water types. *Tellus,* **45A,** 72–79.

——, and E. Tzipermann, 1992: Rates of water mass formation in the North Atlantic Ocean. *J. Phys. Oceanogr.,* **22,** 93–104.

Swift, D. J. P., and K. Aagaard, 1981: Seasonal transitions and water mass formation in the Iceland and Greenland Seas. *Deep-Sea Res.,* **28,** 1107–1129.

Swift, J. H., K. Aagaard, and S.-A. Malmberg, 1980: The contribution of the Denmark Strait overflow to the deep North Atlantic. *Deep-Sea Res.,* **27,** 29–42.

Talley, L. D., and M. S. McCartney, 1982: Distribution and circulation of Labrador Sea Water. *J. Phys. Oceanogr.,* **12,** 1189–1205.

Taylor, H. W., A. L. Gordon, and E. Molinelli, 1978: Climatic characteristics of the Antarctic Polar Front Zone. *J. Geophys. Res.,* **83,** 4572–4578.

Tziperman, E., 1986: On the role of interior mixing and air–sea fluxes in determining the stratification and circulation of the oceans. *J. Phys. Oceanogr.,* **16,** 680–693.

——, and K. Speer, 1994: A study of water mass transformation in the Mediterranean Sea: Analysis of climatological data and a simple 3-box model. *Dyn. Atmos. Oceans,* **21,** 53–82.

Walin, G., 1982: On the relation between sea-surface heat flow and thermal circulation in the ocean. *Tellus,* **34,** 187–195.

Woodruff, S. D., R. J. Slutz, R. L. Jenne, and P. M. Steurer, 1987: A comprehensive ocean–atmosphere data set. *Bull. Amer. Meteor. Soc.,* **68,** 521–527.

Worthington, L. V., 1976: On the North Atlantic Circulation. *The Johns Hopkins Oceanographic Studies,* No. 6, Johns Hopkins University Press, 110 pp.

——, 1981: The water masses of the World Ocean: Some results of a fine-scale census. *Evolution of Physical Oceanography, Scientific Surveys in Honor of Henry Stommel,* B. A. Warren and C. Wunsch, Eds., The MIT Press, 623 pp.

Wright, P., 1988: An atlas based on the COADS data set: Fields of mean wind, cloudiness, and humidity at the surface of the global ocean. Max Plank Institute Report, No. 14, Hamburg, 70 pp.